HAL open science

High-pressure behavior of heteroepitaxial core-shell particles made of Prussian blue analogs

Isabelle Maurin, Miho Itoi, John Cain, Daniel Talham, Thierry Gacoin, Kamel Boukheddaden, Jean-Paul Itié

To cite this version:

Isabelle Maurin, Miho Itoi, John Cain, Daniel Talham, Thierry Gacoin, et al.. High-pressure behavior of heteroepitaxial core-shell particles made of Prussian blue analogs. Journal of Applied Physics, 2021, 129 (23), pp.235106. 10.1063/5.0049223 . hal-03286022

HAL Id: hal-03286022

https://hal.science/hal-03286022v1

Submitted on 5 Nov 2021

HAL is a multi-disciplinary open access archive for the deposit and dissemination of scientific research documents, whether they are published or not. The documents may come from teaching and research institutions in France or abroad, or from public or private research centers.

L'archive ouverte pluridisciplinaire **HAL**, est destinée au dépôt et à la diffusion de documents scientifiques de niveau recherche, publiés ou non, émanant des établissements d'enseignement et de recherche français ou étrangers, des laboratoires publics ou privés.

ACCEPTED MANUSCRIPT

Journal of Applied Physics

This is the author's peer reviewed, accepted manuscript. However, the online version of record will be different from this version once it has been copyedited and typeset.
PLEASE CITE THIS ARTICLE AS DOI: 10.1063/5.0049223

High-pressure behavior of heteroepitaxial core-shell particles made of Prussian blue analogues

Isabelle Maurin,[*1,2] Miho Itoi,[*3] John M. Cain,[4] Daniel R. Talham,[*4] Thierry Gacoin,[1] Kamel Boukheddaden[5] and Jean-Paul Itié[6]

[1] *Physique de la Matière Condensée, UMR 7643, Ecole polytechnique, CNRS, IP Paris, 91128 Palaiseau, France*

[2] *Univ. Grenoble Alpes, CNRS, Grenoble INP, Institut NEEL, BP 166, 38042 Grenoble, France*

[3] *Division of Physics, Institute of Liberal Education, Nihon University School of Medicine, Itabashi-Ku, Tokyo 173-8610, Japan*

[4] *Department of Chemistry, University of Florida, Gainesville, FL 32611-7200, USA*

[5] *Groupe d'Etudes de la Matière Condensée, UMR 8635, CNRS, Université de Versailles-Saint-Quentin 45, Avenue des Etats-Unis, 78035 Versailles cedex, France.*

[6] *Synchrotron SOLEIL, L'orme des Merisiers, Saint Aubin BP 48, 91192 Gif sur Yvette, France.*

[*] *Corresponding authors:*
I. Maurin (isabelle.maurin@neel.cnrs.fr)
M. Itoi (itoi.miho@nihon-u.ac.jp)
D.R. Talham (talham@ufl.edu)

ABSTRACT We report the compressibility of two Prussian blue analogues (PBA) under hydrostatic pressure, one with small and one with relatively large cubic unit cell among PBAs, and investigate the modification of their elastic properties when the two lattices are coupled within a heteroepitaxial core-shell structure. Bulk modulus (K_0) values are derived from x-ray powder diffraction experiments using a diamond anvil cell with silicone oil as pressure-transmitting medium. The pressure-volume curves fitted to Murnaghan equations of states show that K_0 inversely scales with the crystal packing for the rubidium cobalt hexacyanoferrate and rubidium nickel hexacyanochromate samples (K_0 ~ 29 GPa for Co-Fe PBA, a_0 = 9.95 Å and ~ 20 GPa for Ni-Cr PBA, a_0 = 10.48 Å with a_0 the lattice constant at ambient pressure). The two single-phase samples undergo a cubic-to-rhombohedral phase transition above ~ 0.8 GPa, which correlates fairly well with the build-up of nonhydrostatic pressure contributions in the cell. Within the core-shell structure, the volume change observed for the core scales with that of the shell because of the configuration close to the case of a solid pressure-transmitting medium. The Ni-Cr PBA shell layer exhibits an increased rhombohedral distortion with respect to the single-phase reference possibly associated with shearing at the core-shell interface. Its bulk modulus is not significantly modified with respect to that of the single-phase sample despite the presence of defects associated with the growth mode, whereas the *P-V* curve of the core suggests a stiffening of the Co-Fe PBA lattice.

INTRODUCTION

Large photo-induced magnetic changes under visible light in Prussian blue derivatives and other cyanometallate network solids[1-4] have extended the possibility of remote and wireless magnetization control to molecular-based materials. An important issue is that these photo-effects are restricted to very few examples and low temperatures in magnetically-ordered structures.[5] Until now, rationalized approaches to develop single-phase molecular materials that exhibit a persistent magnetization change at, or close to, room temperature in response to light have failed. Efforts undertaken over the last ten years to overcome this issue rely on the design of artificial structures coupling photostrictive and magnetostrictive properties.[6-11] In that sense, these architectures mimic metamaterials or extrinsic magnetoelectrics based on laminates or epitaxial layers.[12,13] The magnetic properties of these composite materials can be controlled by light irradiation making use of the deformation of the photoactive compound to generate mechanical stresses onto the piezomagnetic subsystem.

Several works have detailed these strategies using Prussian blue analogues (PBAs) in layered structures[6] or core-shell particles combining a photoactive cobalt hexacyanoferrate (Co-Fe PBA) core embedded into a ferromagnetic nickel hexacyanochromate (Ni-Cr PBA) shell.[7,9,11] The active component, of general formula $A_xCo[Fe(CN)_6]_y.\ zH_2O$ (A: alkali metal ion), undergoes a charge transfer coupled to a spin transition (termed CTIST throughout earlier literature) triggered by light irradiation in the visible range. This charge transfer between Fe and Co nearest neighbors, $Co^{3+}(LS) - Fe^{2+}(LS) \rightarrow Co^{2+}(HS) - Fe^{3+}(LS)$ (HS/LS: high/low spin) causes an elongation of the unit cell parameter by 3.4% for several compositions.[8, 14, 15] In core-shell architectures, the photoexpansion of the core lattice was shown to produce relatively large static strains, ϵ~0.8%, in the Ni-Cr PBA shell layer.[16,17] This approach was extended to other ferro or ferrimagnetic compounds, Co-Cr PBA[8a] and Cr-Cr PBA with photomagnetic effects that persist up to 125 K and which are now limited by the decay temperature of the photoactive compound.[8b]

Experimental studies have explored optimal configurations for such strain-mediated magnetic switching, mostly focusing on the impact of the shell thickness or of the core size that were shown to control the mechanical counter-action of the shell on the photo-expansion of the core lattice[10,16] and the length scale over which the deformation propagates in the magnetic layer[8a,16,18]. Several requirements could be considered as mandatory for an efficient elastic coupling within the heterostructure, among them the quality of the interface[6a,16] in terms of roughness, chemical intermixing or defect density such as misfit dislocations formed to accommodate different lattice constants across the interface. Differences of thermal expansion for the two subsystems is generally not a key issue as illustrated by several studies, in which the photoactive core actually undergoes a CTIST upon cooling inducing large strains in the shell layer that are relieved under illumination.[8,16,19] Finally, the magnetostrictive subsystem should exhibit larger or at least comparable compressibility than the photostrictive compound. This latter issue is addressed in the current study from high-pressure experiments carried out for cobalt hexacyanoferrate and nickel hexacyanochromate compounds by means of *in situ* powder x-ray diffraction (PXRD), investigating the extent to which these elastic properties are modified in core-shell architectures.

ACCEPTED MANUSCRIPT
Journal of Applied Physics
AIP Publishing
This is the author's peer reviewed, accepted manuscript. However, the online version of record will be different from this version once it has been copyedited and typeset.
PLEASE CITE THIS ARTICLE AS DOI: 10.1063/5.0049223

II. EXPERIMENTAL SECTION

Three PBA samples were synthesized using standard coprecipitation methods. Sample **1** is composed of $Rb_{0.6}Co[Fe(CN)_6]_{0.8}.\ zH_2O$ particles (abbreviated as RbCoFe) that were obtained in two steps by reacting aqueous solutions of $RbNO_3$, $Co(NO_3)_2$ and $K_3Fe(CN)_6$ as detailed in ref 16. After removal of unreacted species, these particles were used as seeds for the growth of a $Rb_{0.2}Ni[Cr(CN)_6]_{0.8}.\ z'H_2O$ shell following well-established procedures, [10,17,20] that lead to RbCoFe@RbNiCr core-shell particles (sample **2**) without side nucleation of extra RbNiCr particles in the reaction bath. A RbNiCr reference sample made of $Rb_{0.2}Ni[Cr(CN)_6]_{0.8}.\ z'H_2O$ particles (**3**) was also prepared as detailed in the supporting information of ref 10. This protocol, adapted from the work of Catala *et al.*,[21] allows the formation of particles with a reduced size dispersion by comparison to standard coprecipitation involving drop-by-drop mixing of the $NiCl_2$, RbCl and $K_3Cr(CN)_6$ precursors.

The dimension of the core particles and the shell thickness were derived from size histograms obtained by Scanning Electron Microscopy using a Hitachi S4800 FEG-SEM equipped for x-ray Energy Dispersive Spectrometry (EDS). Transmission electron microscopy provided complementary images (Philips CM30 microscope operating at 300 kV). The composition of the bare core particles and that of the RbNiCr reference sample were determined from atomic ratios between the metal cations using EDS K lines (Cr, Fe, Co, Ni) and/or L lines (Rb element). These analyses yield Fe/Co = 0.85 ± 0.02 and Rb/Co = 0.60 ± 0.06 for sample **1** and Cr/Ni = 0.75 ± 0.01 and Rb/Ni = 0.16 ± 0.02 for **3**. In the case of core-shell particles (**2**), the overall composition was first obtained by EDS and the chemical formula of the shell layer was derived assuming no intermixing: Fe/Co = 0.82 ± 0.01, Cr/Ni = 0.76 ± 0.02 and Ni/Co = 1.14 ± 0.04. As the two PBAs exhibit different fractions of metallocyanide vacancies and alkali metal ions, we expect that their respective water contents, z and z', differ, with water molecules present both in the sub-octants of the face-centered cubic structure or coordinated to the Co and Ni ions when adjacent to cyanometallate vacancies.[22] Powder x-ray diffraction (PXRD) patterns were collected at room temperature using a PANalytical X'Pert diffractometer equipped with a rear-side graphite monochromator (Cu Kα radiation, λ= 1.5419 Å). Unit-cell analysis was systematically performed from single peak fitting to Pseudo-Voigt (PV) functions and least-square refinement of the interspacing distances. The instrumental resolution function was obtained from a LaB_6 NIST standard (SRM 660a).

PXRD measurements under variable pressure were carried out at the PSICHE workstation (SOLEIL synchrotron facility, France) using a same membrane-diamond anvil cell (DAC, LeToullec-type[23]) for the three samples. 200 µm-diameter holes were drilled in pre-indented stainless steel gaskets of ~ 45 µm initial thickness to load the powder samples. Chemically-inert silicone oil (Prolabo, Rhodorsil 47V1000) was used as pressure-transmitting medium to prevent a dehydration of the samples as the hydration level of PBAs was recently shown to have an influence on their elastic properties.[24,25] Data were collected in transmission geometry at room temperature and constant wavelength (λ= 0.4523 Å, beam size: H×V = 100×40 µm^2 full width at half maximum). We used a 345 mm-diameter Mar Research image plate with 2 to 5 min exposure time and ± 5° rocking of the DAC. One-dimensional diffraction patterns were extracted by integration using the GSAS-2 software.[26] A CeO_2 powder NIST standard (SRM 674a, a = 5.41165 Å) was used to calibrate the sample-to-detector distance (ca. 265 mm), beam center and tilt angle of the 2D detector. Integrated files were corrected from an *adhoc* 4th order polynomial function determined from the CeO_2 NIST calibrant, see Fig. S1 of supplementary material. To improve correction at low 2θ angles, this dataset was completed using laboratory PXRD measurements for the Ni-Cr PBA reference (**3**). For RbNiCr (sample **3**), pressure changes were monitored from the fluorescence of Cr^{3+}-doped Al_2O_3 (ruby) spheres and the shift of the R1 spectral line (at ~ 693.2 nm).[27] The typical error on the pressure values is ± 0.1 GPa.[28] An alternative pressure gauge was used for samples **1** and **2** that are both composed of $Rb_{0.6}Co[Fe(CN)_6]_{0.8}.\ zH_2O$ particles. For these two samples, we observed an irreversible structural transformation of the RbCoFe lattice when the powder was illuminated by the laser used for the excitation of the ruby luminescence (530 nm, 10 mW), that may be associated with large photo-thermal effects. For samples **1** and **2**, additional sets of PXRD measurements were thus collected using gold as an internal pressure calibrant and the tabulated Au compressibility determined by Heinz and Jeanloz.[29]

III. RESULTS AND DISCUSSION

Pressure changes within coupled $Rb_{0.6}Co[Fe(CN)_6]_{0.8}.\ zH_2O$ (RbCoFe) and $Rb_{0.2}Ni[Cr(CN)_6]_{0.8}.\ z'H_2O$ (RbNiCr) lattices were investigated by comparing the pressure-response of a RbCoFe@RbNiCr core-shell structure to those of RbCoFe and RbNiCr single-phase samples. The RbCoFe core particles were synthesized in two steps, through a first coprecipitation yielding about 95-100 nm particles followed by a second growth step to increase their size to ~ 140 nm (Fig. 1(a)). After purification, a portion of these particles were recovered as powder and used as the RbCoFe reference material, while the rest was redispersed and used as primary seeds to grow RbCoFe@RbNiCr particles with a 17 nm thick shell (see Fig. 1(b) and Fig. S2(a) for size distributions). The RbNiCr reference sample (**3**) was synthesized, with a mean particle size of ~ 35 nm, *i.e.* close to the shell thickness in the RbCoFe@RbNiCr heterostructure (Fig. 1(c) and S2(b)). Relative size can be important in this regard as was shown for structurally related Ni-Fe PBA particles, where a stiffening of the lattice when decreasing particle size was attributed to a change of the valence state of surface metallocyanide entities.[30] Representative TEM images of the three samples are presented in Fig. 1, along with PXRD patterns at ambient pressure. The procedure used for the core synthesis typically yields monocrystalline RbCoFe particles of cubo-octahedral shape with (100) planes as terminal facets.[17] Earlier work showed that the RbNiCr shell grows in epitaxy over these cores with the [001](001)RbNiCr//[001](001)RbCoFe relationships.[10]

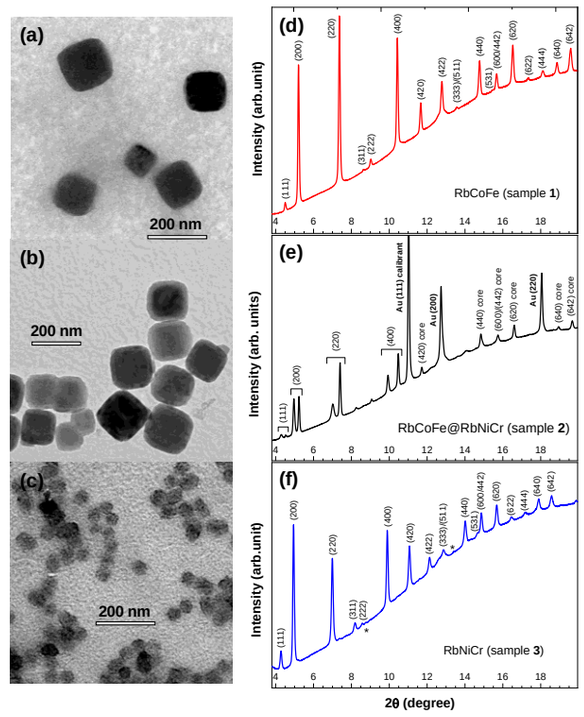

FIG 1. (a-c) TEM images representative of RbCoFe primary particles (**1**), RbCoFe@RbNiCr core-shell particles (**2**) and the RbNiCr reference sample (**3**) ; (d-f) Synchrotron x-ray diffraction profiles recorded at ambient

ACCEPTED MANUSCRIPT
Journal of Applied Physics
AIP Publishing
This is the author's peer reviewed, accepted manuscript. However, the online version of record will be different from this version once it has been copyedited and typeset.
PLEASE CITE THIS ARTICLE AS DOI: 10.1063/5.0049223

pressure for these three samples. Note that the peaks marked by asterisks in (f) comes from an insufficient erase of the image plate. They are absent from consecutive images and also from PXRD data collected for the characterization of the raw powders after synthesis. The broad band at ~12.8° corresponds to a contribution of the gasket.

The two reference samples adopt the face centered cubic structure known for the parent Prussian blue compound $Fe[Fe(CN)_6]_{0.75}.\ 3H_2O$, with Bragg reflections that can be indexed in the $Fm\bar{3}m$ space group. Lattice constants were derived from a least-square refinement of the interspacing distances. We found 10.486(5) Å for the Ni-Cr PBA sample and 9.944(5) Å for the Co-Fe PBA. These values are only slightly modified in the core-shell architecture, *eg.* 10.487(5) Å and 9.933(5) Å, respectively. Determination of the coherence length through whole-profile fitting[31] yields values close to the mean dimension of the particles in the case of the single-phase samples. For the core-shell particles, the lateral size of the shell crystallites was evaluated as ~30 nm from the width of the (200) Bragg reflection assuming platelet-like grains with a height equal to the shell thickness (see ref 10 for details).

A. Pressure-dependence for the single-phase samples

PXRD patterns of samples **1** and **3** were recorded at room temperature while increasing the pressure up to 5 GPa. The evolution of selected diffraction peaks is displayed in Fig. 2(a) and 2(b) for the Co-Fe and Ni-Cr PBAs, respectively. All Bragg reflections shift to higher 2θ, indicating a gradual contraction of the lattice for the two samples. Fig. 3 shows the pressure dependence of the lattice constant, *a*, which was evaluated assuming a cubic unit cell and taking the average of all *a*-values calculated from single peaks, each one fitted to a PV function.

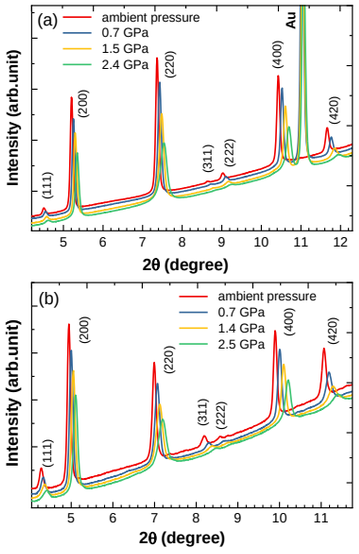

FIG 2. Evolution of selected Bragg reflections under pressure for the 140 nm Co-Fe PBA particles (sample **1**, a) and the 35 nm Ni-Cr PBA particles (**3**, b) indexed in the $Fm\bar{3}m$ space group. The PXRD peak marked as Au corresponds to the pressure gauge.

For the two PBA samples, there is a significant discrepancy above 0.8 GPa when *a*-values determined from individual peaks are compared, with a standard deviation that increases with pressure. Fig. S3 shows that differences are largest when calculations involve (*h*00) reflections, with values that differ by 0.022 Å from those obtained using all other (*hkl*) peaks at 1.8 GPa. Part of this dispersion in the measured *a*-values is explained by nonhydrostatic pressure conditions and the existence of a uniaxial stress component. Under these conditions, Singh and coworkers have shown that the measured *d*-spacing deviates from the hydrostatic value with a (*hkl*) dependence:[32,33]

$$d_m(hkl) = d_p(hkl)[1 + (1 - 3sin^2\theta)Q(hkl)] \qquad \text{eq. (1)}$$

d_p represents the *d*-spacing value corresponding to the hydrostatic component of the stress field, and

$$Q(hkl) = (t/3)[2G^X(hkl)]^{-1} \qquad \text{eq. (2)}$$

where t quantifies the uniaxial stress. $t = (\sigma_3 - \sigma_1)$ is expected to be positive, with σ_3 and σ_1 the stress components in the axial and radial directions, respectively. $G^X(hkl)$ denotes the diffraction shear modulus[34] for the (*hkl*) set of planes. It can be described as a weighted sum of the shear modulus values under the two extreme assumptions of stress continuity ($\alpha = 1$, Reuss-limit, $G_R^X(hkl)$) or strain continuity ($\alpha = 0$, Voigt-limit, $G(V)$) across grain boundaries in aggregates or polycrystalline powders:

$$[2G^X(hkl)]^{-1} = \alpha[2G_R^X(hkl)]^{-1} + (1-\alpha)[2G(V)]^{-1} \qquad \text{eq. (3)}$$

A full description of the parameters and their dependence with the compliance coefficients is given as Supplementary material in the case of cubic symmetry. Note that eq. (1) is only valid for the configuration used, where the load axis coincides with that of the incident x-ray beam.

As $[2G_R^X(hkl)]^{-1}$ can be written as a constant times Γ_{hkl}, with

$$\Gamma(hkl) = [h^2k^2 + k^2l^2 + l^2h^2]/[h^2 + k^2 + l^2]^2 \qquad \text{eq. (4)}$$

the d_m-value is expected to vary linearly with $(1 - 3sin^2\theta)\Gamma(hkl)$. Extraction of the $d_p(hkl)$ values requires either measurements by varying the angle between the load axis and the direction of the incident x-rays[32] or else a preliminary knowledge of the compliance tensor for the compound under study.

For the two PBA samples and the gold calibrant, Γ-plots, *i.e.* $a_m(hkl)$ vs. $3(1 - 3sin^2\theta)\Gamma_{hkl}$ plots, are displayed in Fig. S4 for a direct comparison with Fig. S3. They show a decreased dispersion around a straight line, even for the Au gauge. Analysis in the frame of the Reuss (iso-stress, $\alpha = 1$) model[35] provides an estimate of the uniaxial stress component and its variation as a function of the nominal pressure. Note that this model, which assumes the continuity of the stress field across grain boundaries is presumably valid for weakly bounded monocrystalline PBA particles, but will only provide a lower bound of *t* in the case of gold. Following a procedure identical to that described in ref 36, which is based on the use of tabulated C_{ij} values for gold and their pressure dependence,[37,38] we estimated the uniaxial stress *t* to be 0.10(1) GPa at 1.8 GPa nominal pressure, see Table S1 for a complete set of *t*-values during a compressive run. This uniaxial stress may result from pressure-induced structural modifications of silicone oil or from bridging effects (i.e. grain to grain contacts from an anvil to the other). Nevertheless, one should bear in mind that this uniaxial component was calculated from the gauge and not at the sample location in DAC, so that it should be considered as an approximate of the stress gradient experienced by the PBA samples.

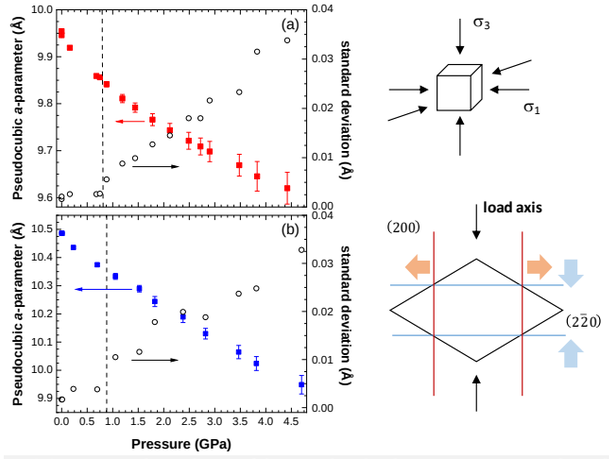

FIG 3. Pressure dependence of the pseudocubic lattice parameter evaluated from the most intense peaks, *i.e.* 12 at low pressures and 7 peaks at 5 GPa for the Co-Fe PBA (sample **1**, a), and from 12 to 5 peaks for the Ni-Cr PBA (sample **3**, b). Error bars correspond to the standard deviation between *a*-values. For comparison, this standard deviation reaches a maximum of 0.002 Å for the gold gauge. On the right-hand side, schematics used to

ACCEPTED MANUSCRIPT
Journal of Applied Physics
AIP Publishing
This is the author's peer reviewed, accepted manuscript. However, the online version of record will be different from this version once it has been copyedited and typeset.
PLEASE CITE THIS ARTICLE AS DOI: 10.1063/5.0049223

define the radial (σ_1) and axial (σ_3) components of the applied stress and 2D illustration of the distortion along the load axis. With these notations, the uniaxial stress writes as $t = (\sigma_3 - \sigma_1)$ while the hydrostatic pressure component is $\sigma_p = (\sigma_1 + t/3)$.

The striking feature is the positive slope of the Γ-plots in the case of the two PBAs, which either suggests a more complex stress field in the experimental volume leading to large differential stress even along the radial direction of the DAC or else a specific response of the PBA lattices, similar to that of auxetic materials, with a positive strain along specific directions when the sample is compressed. Note that auxetic behaviors are usually observed when several deformation modes compete like in the case of solids with strongly directional bondings, such as silicates and aluminosilicates[39,40] with a hinge-like structure susceptible to flex.

Prussian blue analogues exhibit a double perovskite structure based on alternate octahedral units connected by vertices in 3D. In these compounds, octahedra tilts under compressive stress have been suggested from several spectroscopic studies,[41,42,43] and a phase transition driven by cooperative tilting was recently evidenced from single-crystal structure determination for $Mn[Co(CN)_6]_{0.67}.zH_2O$.[24] For this compound, Boström *et al.* reported a pressure-induced structural transition with symmetry lowering from $Fm\bar{3}m$ to $R\bar{3}$ space group. A similar rhombohedral distortion was observed upon alkali ion exchange in cobalt hexacyanoferrates,[44] with a slight deviation from 90° of the dihedral angles between unit cell vectors, that was associated to the difference in ionic radii of the Na^+ and K^+ ions with respect to sub-octants voids. This symmetry lowering led to a well-resolved line splitting of the non (h00) reflections also mentioned in ref 24. This distortion will also shift non (h00) peaks from their 2θ position with respect to cubic symmetry as depicted in Fig. S5 for the {220} family of lattice planes. This shift can be used to evaluate the α_R^* angle, while the position of the unsplit (200) peaks allows a direct measure of a_R^* and a complete description of the rhombohedral lattice in reciprocal space[45] (see the Supplementary material section for details). However in the present geometry, only one of the (220) or $(2\bar{2}0)$ peak is observed as a result of the uniaxial stress component that tend to compress the planes perpendicular to the load axis, here the direction of the incident x-rays, for which the diffraction conditions are not fulfilled, whereas the planes in expansion lying quasi parallel to the load axis contribute to the diffracted signal. This distortion is schematized in Fig. 3. Note that the absence of a significant decrease of the relative intensity of the (200) and $(220)/(2\bar{2}0)$ peaks strongly suggest the development of preferred orientation (texture) that is frequently observed for specimens compressed between opposed anvils. The auxetic-like behavior suggested by the positive slope of the Γ-plots in Fig. S4 could thus be an artifact due to the observation of the only lattice planes in expansion.

Using these rhombohedral settings, we have determined the evolution of the a and α_R-parameters, along with the volume change as a function of pressure for the two PBAs, see Fig. 4. For rhombohedral systems, the volume is expressed as:

$$V_R = a_R^3\sqrt{(1 + 2cos^3\alpha_R - 3cos^2\alpha_R)} \qquad \text{eq. (5)}$$

and will mostly mimic the evolution of a_R for small deviations to cubic symmetry.

We found that α_R decreases linearly with pressure, with nearly superimposable behavior for the two PBAs despite the fact that they exhibit different compositions and cell volume. Fig. 4(b) suggests a correlation between the amplitude of the rhombic distortion quantified here by α_R and the onset of pressure gradients in the DAC. This could also explain why the cubic-to-rhombohedral distortion occurs at similar nominal pressure for the two PBAs, presumably as a result of shearing forces.

While linearity is observed over a large pressure range for the Co-Fe PBA sample, the α_R variation shows a cusp at about 2.5 GPa in the case of Ni-Cr PBA. This threshold pressure was already pointed out by Klotz and coworkers when they tried to assess the hydrostaticity of various pressure-transmitting media using ruby chips dispersed over the area of the gasket aperture.[46] They detected substantial gradients above 3 GPa for Rhodorsil 47V1000, *eg* 0.25 GPa differences at 5 GPa nominal pressure, which were assigned to differential and/or shear stresses due to pressure-induced solidification. In the present datasets, an asymmetry of the peak shape is observed for unsplit (h00) Bragg reflections above 2.5 GPa, which confirms the presence of significant pressure gradients in the gasket.[47] Comparison of the α_R changes for the two PBAs suggest that the nickel hexacyanochromate network is more sensitive to these differential stresses. Above 2.5 GPa, plastic deformation mechanisms may be favored and explain the non reversible behavior of the Ni-Cr PBA particles, as we observe the persistence of a large line broadening and a decrease of the lattice parameter after relieving the pressure from 7 GPa to ambient. In contrast, the Co-Fe PBA sample exhibits a quasi-reversible behavior in the same pressure range.

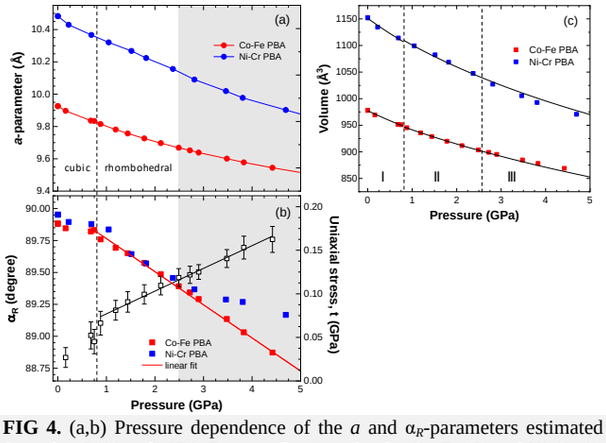

FIG 4. (a,b) Pressure dependence of the a and α_R-parameters estimated from the (200) and (220) Bragg reflections for the Co-Fe (**1**) and Ni-Cr (**3**) PBAs. The red line in (b) is a linear fit in the [0.8-5 GPa] range. The evolution of the uniaxial stress determined from the Au calibrant is shown for comparison. The gray area marks the hydrostaticity limit of Rhodorsil 47V1000 according to ref 46. Volume changes are displayed in (c), with fits to Murnaghan EoS (solid black lines) both in pressure ranges I and II. The fit related to the rhombohedral polymorph is visualized up to 5 GPa. Here, acute α_R angles were assumed to be comparable to ref 24 and 45 ; this corresponds to the stretching of the cubic cell along the [111] 3-fold axis. Note that for such small deviations to cubic symmetry, the choice of obtuse or acute angle for α_R (or α_R^*) does not impact the evaluation of a and V (less than 2×10^{-6} relative change in the two cases).

Because of this hydrostaticity limit, we restricted the analyses of the isothermal pressure-volume curves to 2.5 GPa, and use a Murnaghan equation of state to obtain bulk modulus (K_0) parameters with the first pressure derivative, K_0' fixed to 4 (common values ranging between 3 and 5 for halides, oxides, carbides including molecular solids[45]). The solid lines in Fig. 4(c) correspond to fits of the unit cell volume using EosFit7-GUI,[48] that include uncertainty estimates for the volume and the pressure. Table 1 shows that similar K_0 values are derived for the cubic and the rhombohedral polymorphs in the pressure range [0-0.8 GPa] and [0.8-2.5 GPa], as already observed in the case of $Mn[Co(CN)_6]_{0.67}.zH_2O$.[24] For pressure range II representative of rhombohedral lattices, we found V_0 = 972.2(8) Å^3 and K_0 = 29.0(5) GPa for the Co-Fe PBA sample and V_0 = 1153(4) Å^3, K_0 = 20(1) GPa for Ni-Cr PBA, where V_0 is the volume per formula unit at atmospheric pressure. Note that given the particle sizes, greater than tens of nanometers, we are in a regime well beyond where small particle size was shown to cause lattice stiffening in structurally similar Ni-Fe PBA compositions.[30]

As already discussed by Boström *et al.*, correlating these results to literature data is challenging because of differences in the experimental set-ups including pressure-transmitting media and pressure ranges, differences in the analytical method used to evaluate K_0 and sample variability.[24] As the magnitude of the

ACCEPTED MANUSCRIPT
Journal of Applied Physics
AIP Publishing
This is the author's peer reviewed, accepted manuscript. However, the online version of record will be different from this version once it has been copyedited and typeset.
PLEASE CITE THIS ARTICLE AS DOI: 10.1063/5.0049223

uniaxial stress should largely depend on experiments, we could also wonder whether the distribution of strain states due to nonhydrostatic stress conditions is another source of discrepancy. For instance, an inverse isothermal compressibility $-(dV/VdP)^{-1}$ of 31 GPa was derived from high-pressure neutron diffraction for a potassium nickel hexacyanochromate.[49] In the case of hexacyanoferrates, a large range of K_0 values, from 18 to 71 GPa, have been reported from different techniques.[30,42,45,50] Bleuzen *et al.* found $K_0 \sim 43$ GPa with $K_0' = 3.6$ for $Cs_{0.5}Co[Fe(CN)_6]_{0.8}.\ zH_2O$ from energy dispersive x-ray diffraction in DAC using silicone oil.[45] This sample shows a majority of Co^{3+}-NC-Fe^{2+} linkages like the RbCoFe particles of the present study, and a same fraction of $[Fe(CN)_6]$ vacancies. The substitution of Cs by Rb presumably accounts for the large difference in K_0 values for the two Co-Fe PBAs as these studies used close PXRD set-ups and a same Murnaghan EoS for fitting. This conclusion is in good agreement with a recent investigation comparing rubidium and cesium Mn-Co PBA,[25] but the impact of specific arrangements of the metallocyanide vacancies[51] as well as variations in the hydration level[25] between the two Co-Fe PBA samples cannot be discarded. Besides, the alkali ion and its relative content could play a crucial role in the rhombohedral distortion according to former studies based on alkali-ion exchange[44] or phase transformations involving a large volume change.[52]

	Mean size (nm)	*Standard deviation* (nm)	K_0^I (GPa)	K_0^{II} (GPa)
Co-Fe PBA (**1**)	142	24	25(1)	29.0(5)
Ni-Cr PBA (**3**)	33	4	19(2)	20(1)
RbCoFe@RbNiCr (**2**)	176	29		
RbCoFe core in (**2**)			-	45.0(8)
RbNiCr shell in (**2**)			-	20.8(7)

TABLE 1. Mean size and standard deviation of the size distributions (from SEM images for **1** and **2**, and TEM for **3**). Bulk modulus values, K_0^I and K_0^{II}, obtained from fits of *P-V* curves to Murnaghan EoS in the pressure range I [0-0.8 GPa] and II [0.8-2.5 GPa]. Take note of the large uncertainties on K_0^I due to the limited pressure range over which the fit is performed, and the low number of data points. As a result, these latter values should be taken with caution.

Nevertheless, from this self-consistent study, we can conclude to a significantly larger compressibility of the rubidium hexacyanochromate compound with respect the rubidium hexacyanoferrate used as core in the heterostructure sample. This corresponds to a configuration favorable to the elastic coupling, as we can anticipate a decreased mechanical counteraction of the shell on the volume changes experienced by the core lattice during CTIST from numerical simulations.[53]

B. Comparison with the core-shell architecture

Core-shell heterostructures can be considered as an experimental platform to rationalize how differences in bulk moduli influences the transfer of strain across the interface by varying the chemical composition of the shell and/or core components. In the context of this study, they can also be used to address the question of the impact of epitaxial growth on the elastic properties of layered materials, and on the amplitude of the rhombohedral distortions.

For RbCoFe@RbNiCr particles (sample **2**), PXRD data indicate the coexistence of two well separated *fcc* lattices, with patterns close to those of the single-phase compounds (see Fig. 1). The rather large mismatch of 5.3% between the two nominal lattices favors the absence of pseudomorphic overlay and a 3D growth mode of the shell layer with a misfit accommodated through the formation of both dislocations and grain boundaries (see ref 10 for a description of the growth of these heterostructures). The evolution of selected diffraction peaks during a compressive run is displayed in Fig. 5(a). The overall volume change and the α_R-pressure dependence are reported in Fig. 5(b) and 5(c) respectively, together with the variations found for the single-phase samples. Analyses were performed in the [0.8-2.5 GPa] range for a direct comparison with the single-phase materials, see Table 1 for the K_0-parameters extracted for the core and shell contributions. The reduced number of pressure points below 1 GPa impedes any reliable analyses.

In the core-shell structure, the RbNiCr shell layer contracts as in the reference materials despite the presence of a stiffer RbCoFe inner core lattice. For a rather large volume ratio between the core and the shell (of the order of 0.75), no strain hardening is observed as a result of epitaxial growth, nor a largely increased compressibility because of a network of misfit and threading dislocations acting as an additional source of structural flexibility. However, Fig. 5(c) shows a large α_R decrease upon compression that could be explained by reinforced shearing forces due to the interaction with the less compressible core lattice. Deviations to cubic symmetry fall off above 2.5 GPa, with comparable *a*-values determined from (200) and (220) reflections, suggesting that the large defect densities associated with the growth mode of the shell favor plastic mechanisms and/or suppress the long-range correlations required for a cooperative tilting of the polyhedral units if associated with the rhombohedral distortion.

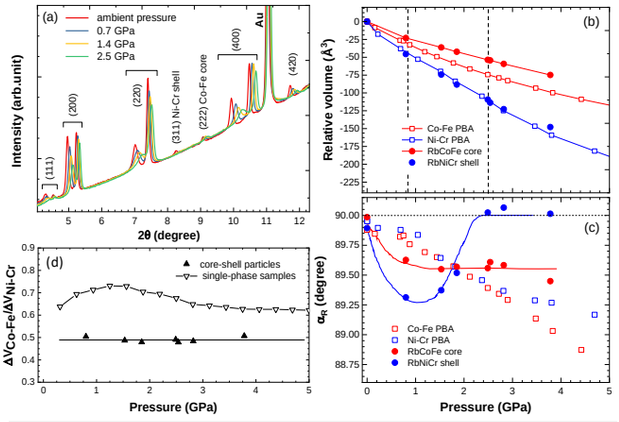

FIG 5. (a) X-ray diffraction profiles of the RbCoFe@RbNiCr particles (sample **2**) at variable pressures. The PXRD peak marked as Au corresponds to the pressure gauge. (b-c) Volume changes calculated from *a* and α_R-values for the different lattices as single-phase materials or within the core-shell structure, red and blue symbols. Lines are just guide to the eye. (d) The ratio $\Delta V_{Co\text{-}Fe}/\Delta V_{Ni\text{-}Cr}$ in the composite is compared to the behavior as separate constituents.

For the RbCoFe core lattice, the striking feature is a significantly decreased volume change, associated with a weaker amplitude of α_R variation, see Fig. 5(c). However, the *apparent* K_0 value of 45 GPa is partly explained by the fact that the core is surrounded by a softer shell matrix, that deforms first, in analogy with pyrophillite-based pressure cells associated to cubic anvils. Indeed, when plotting the ratio $\Delta V_{Co\text{-}Fe}/\Delta V_{Ni\text{-}Cr}$ as a function of the nominal pressure, we find a constant (0.49 ± 0.01) as opposed to the variation observed when comparing the single-phase materials (Fig. 5(d)). We can thus estimate the *real* K_0-value for the core part in the [0.8-2.5 GPa] range:

$$\left(\Delta V^{core}/V_0^{core}\right) = 0.49\left(\Delta V^{shell}/V_0^{shell}\right)\left(V_0^{shell}/V_0^{core}\right) \sim 0.49\left(1/K_0^{shell}\right)\left(V_0^{shell}/V_0^{core}\right)P$$

By assimilating the last term to $\left(1/K_0^{core}\right)P$, we obtain $K_0^{core} \sim$ 35(2) GPa, which is larger than the value found for the bare particles and suggests some stiffening of the core lattice in the presence of the shell. This would further increase the difference in compressibility of the two lattices, but also affect the cooperative character of the spin transition for the core component according to simulations,[53] pressure studies related to spin-crossover (SCO) solids[54] or experiments related to SCO particles embedded in shells of variable stiffness.[55]

This study provides quantitative values of the elastic constants and how much they get modified in core-shell architectures. It should

ACCEPTED MANUSCRIPT
Journal of Applied Physics
AIP Publishing
This is the author's peer reviewed, accepted manuscript. However, the online version of record will be different from this version once it has been copyedited and typeset.
PLEASE CITE THIS ARTICLE AS DOI: 10.1063/5.0049223

now be extended to core-shell structures with reduced lattice mismatch, where we anticipate (i) pseudomorphic growth closer to the case study of numerical simulations, and (ii) stronger mechanical coupling. At present, most theoretical investigations treat separately the influence of the lattice misfit and differences in stiffness on the thermal, mechanical and even temporal-response of such heteroepitaxial layers,[53,56] while these two parameters may be coupled. At last, note that for the RbCoFe cores the nearly constant α_R-evolution after setting up the first pressure value mimics again the evolution of the uniaxial stress component determined from the gold gauge (see the Supplementary material).

C. Impact of inhomogeneous stress fields

These measurements suggest that PBA network solids are sensitive to the build-up of small stress gradients in the DAC that can be difficult to detect from alternative probes, such as ruby fluorescence lines that remain sharp in the presence of uniaxial stress[57] or the evolution of crystalline pressure gauges. A fair indicator for the maximum tolerable pressure gradient for an accurate determination of lattice parameters is $\Delta P < K_0\epsilon$,[46] with K_0 the bulk modulus of the sample and ϵ the relative error on d-spacings. ϵ is typically of the order of 10^{-3} for high-pressure synchrotron diffraction measurements. Considering the range of K_0-values given in the literature for PBAs and other cyanometallate network solids,[24,25,30,45,49] pressure gradients should not exceed 0.02 GPa while this criteria relaxes to ~0.17 GPa for gold. However, comparison between the single-phase Ni-Cr PBA particles and the same compound grown as a shell layer indicates that small rhombic distortion of the cubic cell has little influence on bulk modulus values, so that discrepancies observed in the literature rather reflect sample variability or fitting procedures. Definite conclusions would require systematic studies performed on a same sample batch using different pressure-transmitting media and/or powder amount to investigate the impact of bridging and tune the uniaxial stress on a wider range.

The fact that the elastic properties of PBAs exhibit a significant anisotropy, which makes them prone to rhombohedral distortion and sensitive to inhomogeneous stress fields, may have a large impact on the switching properties of cobalt hexacyanoferrates because of the build-up of internal pressure gradients associated with the large volume change during CTIST. This effect should be emphasized when the optically or thermally-activated transition proceeds through the nucleation and growth of domains within a monocrystalline particle, that is close to the configuration of epitaxially coupled layers even though the crystalline orientation of the interface may differ from that of the core-shell structures. This aspect was recently pointed out in spin-crossover (SCO) solids, as such gradients could be a major ingredient to describe the hysteretic properties of these materials.[58] In the case of PBAs, these distortions may involve correlated tilts of the metallocyanide units, presumably at medium distances due to the inherent structural disorder, and have a large counteraction on the charge transfer processes because of a decrease of the transfer integral.

Understanding the mechanical response of SCO and PBA lattices under non uniform stress is thus important to interpret the results on mechanically-coupled core-shell particles based on photostrictive/magnetostrictive architectures which are assumed to exhibit complex strain/stress fields based on microscopic investigations involving both theoretical and experimental approaches.[17,59] These aspects should also be of importance for matrix crystallization effects that were shown to control the cooperativity of SCO particles,[60] or structure reinforcement upon (de)lithiation in PBA-based cathode materials.[61]

IV. CONCLUSIONS

The large photostriction reported in Prussian blue analogues has been used to design artificial structures coupling photostrictive and magnetostrictive properties and could be further exploited to develop alternative opto-mechanical devices and sensors. For these compounds, most of the phenomena including photophysical properties relies on the elastic properties of the PBA network, but reports on their piezomagnetic properties or of their elastic constants are still limited despite recent efforts[24,25] to rationalize the apparent variability in the literature results.

This study provides new estimates of bulk modulus values under ambient conditions for specific rubidium cobalt hexacyanoferrate and rubidium nickel hexacyanochromate compositions. This work highlights the fact that PBA networks are likely prone to structural distortion under slight deviations to hydrostatic conditions. The core-shell heterostructures are even more susceptible to distortion, possibly because of shearing associated with the core-shell interface. These distortions may have a large impact on the switching properties of photoactive PBA derivatives, even in the absence of external pressure, as the transition involve charge-transfer processes through the CN bridges. This study also suggests a relative stiffening of the core lattice even in the presence of a deformable shell. This last finding as well as the open question of the driving force of the rhombohedral transformation, shearing forces or uniaxial stress, could be further addressed from core-shell structures made of a same core by changing the composition of the shell to tune the lattice mismatch and the mechanical strength between the two solids.

SUPPLEMENTARY MATERIAL

See supplementary material for the correction applied to the integrated PXRD data; $a_m(hkl)$ vs. 2θ or $3(1-3sin^2\theta)\Gamma_{hkl}$ plots; estimation of the uniaxial pressure component from the gold gauge; analyses of the experimental PXRD patterns in terms of rhombohedral distortion.

The data that support the findings of this study are available from the corresponding author upon reasonable request.

ACKNOWLEDGMENTS

The authors acknowledge SOLEIL for provision of synchrotron radiation facilities. M.I. was supported by CNRS (Centre National de la Recherche Scientifique) as invited researcher in 2013. M. Poggi is acknowledged for the TEM observations. This work was supported, in part, by the Division of Materials Research (DMR) at the National Science Foundation (NSF) via DMR-1904596 (D.R.T.)

[1] O. Sato, T. Iyoda, A. Fujishima, and K. Hashimoto. Science **272**, 704 (1996).
[2] S. Ohkoshi, S. Yorozu, O. Sato, T. Iyoda, A. Fujishima, and K. Hashimoto, Appl. Phys. Lett. **70**, 1040 (1997).
[3] H. Tokoro, S. Ohkoshi, and K. Hashimoto. Appl. Phys. Lett. **82**, 1245 (2003).
[4] S.-I. Ohkoshi, N. Machida, Z.J. Zhong, and K. Hashimoto, Synth. Met. **122**, 523 (2001) ; S.-I. Ohkoshi, H. Tokoro, T. Hozumi, Y. Zhang, K. Hashimoto, C. Mathoniere, I. Bord, G. Rombaut, M. Verelst, C. Cartier dit Moulin, and F. Villain, J. Am. Chem. Soc. **128**, 270 (2006).
[5] A.J. Epstein, MRS Bulletin **28**, 492 (2003).
[6] (a) D.M. Pajerowski, M.J. Andrus, J.E. Gardner, E.S. Knowles, M.W. Meisel, and D.R. Talham, J. Am. Chem. Soc. **132**, 4058 (2010); (b) D.M. Pajerowski, J.E. Gardner, F.A. Frye, M.J. Andrus, M.F. Dumont, E.S. Knowles, M.W. Meisel, and D.R. Talham, Chem. Mater. **23**, 3045 (2011).

ACCEPTED MANUSCRIPT
Journal of Applied Physics
AIP Publishing
This is the author's peer reviewed, accepted manuscript. However, the online version of record will be different from this version once it has been copyedited and typeset.
PLEASE CITE THIS ARTICLE AS DOI: 10.1063/5.0049223

[7] M.F. Dumont, E.S. Knowles, A. Guiet, D.M. Pajerowski, A. Gomez, S.W. Kycia, M.W. Meisel, and D.R. Talham, Inorg. Chem. **50**, 4295 (2011).
[8] (a) O.N. Risset, P.A. Quintero, T.V. Brinzari, M.J. Andrus, M.W. Lufaso, M.W. Meisel and D.R. Talham, J. Am. Chem. Soc. **136**, 15660 (2014); (b) O.N. Risset, T.V. Brinzari, M.W. Meisel, and D.R. Talham, Chem. Mater. **27**, 6185 (2015).
[9] N. Dia, L. Lisnard, Y. Prado, A. Gloter, O. Stephan, F. Brisset, H. Hafez, Z. Saad, C. Mathonière, L. Catala, and T. Mallah, Inorg. Chem. **52**, 10264 (2013).
[10] M. Presle, I. Maurin, F. Maroun, R. Cortès, L. Lu, R. Sayed Hassan, E. Larquet, J.-M. Guigner, E. Rivière, J. P. Wright, J.-P. Boilot, and T. Gacoin, J. Phys. Chem. C **118**, 13186 (2014).
[11] C.-H. Lee, M.-Y. Wang, E. Batsaikhan, C.-M. Wu, C.-W. Wang, and W.-H. Li, ACS Omega **2**, 4227 (2017).
[12] G. Srinivasan, E.T. Rasmussen, and R. Hayes, Phys. Rev. B **67**, 014418 (2003).
[13] M. Zhu, T. Nan, B. Peng, Y. Zhang, Z. Zhou, X. Yang, W. Ren, N.X. Sun, and M. Liu, IEEE Trans. Magn. **1**, 99 (2017).
[14] V. Escax, A. Bleuzen, J.P. Itié, P. Munsch, F. Varret, and M. Verdaguer, J. Phys. Chem. B **107**, 4763 (2003).
[15] I. Maurin, D. Chernyshov, F. Varret, A. Bleuzen, H. Tokoro, K. Hashimoto, and S. Ohkoshi. Phys. Rev. B. **79**, 064420 (2009).
[16] A.C. Felts, M.J. Andrus, E.S. Knowles, P.A. Quintero, A.R. Ahir, O.N. Risset, C.H. Li, I. Maurin, G.J. Halder, K.A. Abboud, M.W. Meisel, and D.R. Talham, J. Phys. Chem. C **120**, 5420 (2016).
[17] A. Adam, M. Poggi, E. Larquet, R. Cortès, L. Martinelli, P.-E. Coulon, E. Lahera, O. Proux, D. Chernyshov, K. Boukheddaden, T. Gacoin, and I. Maurin, Nanoscale **10**, 16030 (2018).
[18] J.M. Cain, A.C. Felts, M.W. Meisel, and D.R. Talham, Chem. Mater. **33**, 246 (2021).
[19] A.C. Felts, A. Slimani, J.M. Cain, M.J. Andrus, A.R. Ahir, K.A. Abboud, M.W. Meisel, K. Boukheddaden, and D.R. Talham, J. Am. Chem. Soc. **140**, 5814 (2018).
[20] M. Presle, J. Lemainque, J.M. Guigner, E. Larquet, I. Maurin, J.-P. Boilot, and T. Gacoin, New J. Chem. **35**, 1296 (2011).
[21] Y. Prado, L. Lisnard, D. Heurtaux, G. Rogez, A. Gloter, O. Stephan, N. Dia, E. Riviere, L. Catala, and T. Mallah, Chem. Commun. **47**, 1051 (2011).
[22] F. Herren, P.A. Ludi, and W. Haelg, Inorg. Chem. 19, 956 (1980).
[23] (a) R. LeToullec, J.-P. Pinceaux, and P. Loubeyre, High Press. Res. **1**, 77 (1988). (b) R. Letoullec, J.-P. Pinceaux, and P. Loubeyre, High Press. Res. **5**, 871 (1990).
[24] H.L.B. Boström, I.E. Collings, A.B. Cairns, C. P. Romao, and A.L. Goodwin, Dalton Trans. **48**, 1647 (2019).
[25] H.L.B. Boström, I.E. Collings, D. Daisenberger, C.J. Ridley, N.P Funnell, and A.B. Cairns, J. Am. Chem. Soc. **143**, 3544 (2021).
[26] B.H. Toby, and R.B. Von Dreele, J. Appl. Cryst. **46**, 544 (2013).
[27] H.K. Mao, J. Xu, and P.M. Bell. J. Geophys. Res. **91**, 4673 (1986).
[28] A. Filipponi and A. Di Cicco, Phys. Rev. B **49**, 12564 (1994); J. M. Recio, J. M. Menéndez, and A. O. de la Roza, *An Introduction to High-Pressure Science and Technology*, CRC Press, 2016.
[29] D.L Heinz, and R. Jeanloz, J. Appl. Phys. **55**, 885 (1984).
[30] (a) G. Félix, W. Nicolazzi, L. Salmon, G. Molnár, M. Perrier, G. Maurin, J. Larionova, J. Long, Y. Guari, and A. Bousseksou, Phys. Rev. Lett. **110**, 235701 (2013); (b) G. Félix, M. Mikolasek, H.J. Shepherd, J. Long, J. Larionova, Y. Guari, J.P. Itié, A.I. Chumakov, W. Nicolazzi, G. Molnár and A. Bousseksou, Eur. J. Inorg. Chem. **3-4**, 443 (2018).
[31] J. Rodriguez-Carvajal, Physica B **192**, 55, (1993); http://www.ill.eu/sites/fullprof/index.html.
[32] A.K. Singh, C. Balasingh, H.-K. Mao, R.J. Hemley, and J. Shu, J. Appl. Phys. **83**, 7567 (1998).
[33] A.K. Singh, and K. Takemura, J. Appl. Phys. **90**, 3269 (2001).
[34] X refers to shear modulus obtained from strain measurements using x-ray diffraction that may differ from the one derived from macroscopic techniques such as strain gauge.
[35] A. Reuss, Z. Angew. Math. Mech. **9**, 49 (1929).
[36] K. Takemura, and A. Dewaele, Phys. Rev. B **78**, 104119 (2008).
[37] T.S. Duffy, G. Shen, D.L. Heinz, J. Shu, Y. Ma, H.-K. Mao, R.J. Hemley, and A. K. Singh, Phys. Rev. B **60**, 15063 (1999).
[38] B. Golding, S.C. Moss, and B.L. Averbach, Phys. Rev. **158**, 637 FMatsuda(1967).
[39] A. Yeganeh-Haeri, D.J. Weidner, and J. B. Parise, Science, **257**, 650 (1992).
[40] C. Sanchez-Valle, Z.A. Lethbridge, S.V. Sinogeikin, J.J. Williams, R.I. Walton, K.E. Evans, and J.D. Bass, J. Chem. Phys. **128**, 184503 (2008).
[41] X. Liu, Y. Moritomo, T. Matsuda, H. Kamioka, H. Tokoro, and S.-I. Ohkoshi, J. Phys. Soc. Jpn., **78**, 013602 (2009).
[42] T. Matsuda, X. Liu, T. Shibata, H. Kamioka, Y. Ohishi, and Y. Moritomo, J. Phys. Soc. Jpn., **78**, 105002 (2009).
[43] J.-D. Cafun, J. Lejeune, J.-P. Itié, F. Baudelet, and A. Bleuzen, J. Phys. Chem. C, **117**, 19645 (2013).
[44] T. Matsuda, J. Kim, and Y. Moritomo, J. Am. Chem. Soc. **132**, 12206 (2010).
[45] A. Bleuzen, J.-D. Cafun, A. Bachschmidt, M. Verdaguer, P. Munsch, F. Baudelet, and J.-P. Itié. J. Phys. Chem. C **112**, 17709 (2008).
[46] S. Klotz, J.-C. Chervin, P. Munsch, and G. Le Marchand, J. Phys. D: Appl. Phys. **42**, 075413 (2009).
[47] K. Takemura, J. Appl. Phys. **89**, 662 (2001).
[48] R. J. Angel, M. Alvaro, and J. Gonzalez-Platas, Z. Kristallogr. **229**, 405 (2014) ; J. Gonzalez-Platas, M. Alvaro, F. Nestola, and R. Angel, IUCr, J. Appl. Crystallogr. **49**, 1377 (2016).
[49] D. M. Pajerowski, S. E. Conklin, J. Leao, L. W. Harriger, and D. Phelan, Phys. Rev. B **91**, 094104 (2015).
[50] K. Boukheddaden, E.D. Loutete-Dangui, E. Codjovi, M. Castro, J.A. Rodriguéz-Velamazán, S. Ohkoshi, H. Tokoro, M. Koubaa, Y. Abid, and F. Varret, J. Appl. Phys. **109**, 013520 (2011).
[51] A. Simonov, T. De Baerdemaeker, H.L.B. Boström, M.L. Ríos Gómez, H.J. Gray, D. Chernyshov, A. Bosak, H.-B. Bürgi, and A.L. Goodwin, Nature **578**, 256 (2020).
[52] A. Bleuzen, V. Escax, A. Ferrier, F. Villain, M. Verdaguer, P. Münsch, and J.P. Itié, Angew. Chem. Int. Ed. **43**, 3728 (2004).
[53] A. Slimani, K. Boukheddaden, and K. Yamashita, Phys. Rev. B **89**, 214109 (2014).
[54] (a) E. Codjovi, N. Menéndez, J. Jeftic, and F. Varret, C. R. Acad. Sci. Series IIC-Chem. **4**, 181 (2001); (b) P. Gütlich, A. B. Gaspar, V. Ksenofontov, and Y. Garcia, J. Physics: Condens. Matter **16**, S1087 (2004).
[55] Y. Raza, F. Volatron, S. Moldovan, O. Ersen, V. Huc, C. Martini, F. Brisset, A. Gloter, O. Stephan, A. Bousseksou, L. Catala, and T. Mallah, Chem. Commun. 47, 11501 (2011).
[56] (a) A. Slimani, and K. Boukheddaden, Phys. Chem. Chem. Phys., 20, 28583 (2018); (b) K. Affes, A. Slimani, A. Maalej, and K. Boukheddaden, Chem. Phys. Lett. **718**, 46 (2019).
[57] M. Chai, and J. M. Brown, Geophys. Res. Lett. **23**, 3539 (1996).
[58] I. Rusu, I. C. Manolache-Rusu, A. Diaconu, O. Palamarciuc, I. A. Gural'skiy, G. Molnar, and A. Rotaru, J. Appl. Phys. **129**, 064501 (2021).
[59] H. Oubouchou, A. Slimani, and K. Boukheddaden, Phys. Rev. B **87**, 104104 (2013).
[60] J. Laisney, D. Morineau, C. Enachescu, R. Tanasa, E. Rivière, R. Guillot, and M.-L. Boillot, J. Mater. Chem. C **8**,3 7067 (2020).
[61] C.H. Li, M.K. Peprah, D. Asakura, M.W. Meisel, M. Okubo, and D.R. Talham, Chem. Mater. **275**, 1524 (2015).

AIP Publishing

Journal of Applied Physics

ACCEPTED MANUSCRIPT

This is the author's peer reviewed, accepted manuscript. However, the online version of record will be different from this version once it has been copyedited and typeset.

PLEASE CITE THIS ARTICLE AS DOI: 10.1063/5.0049[illegible]

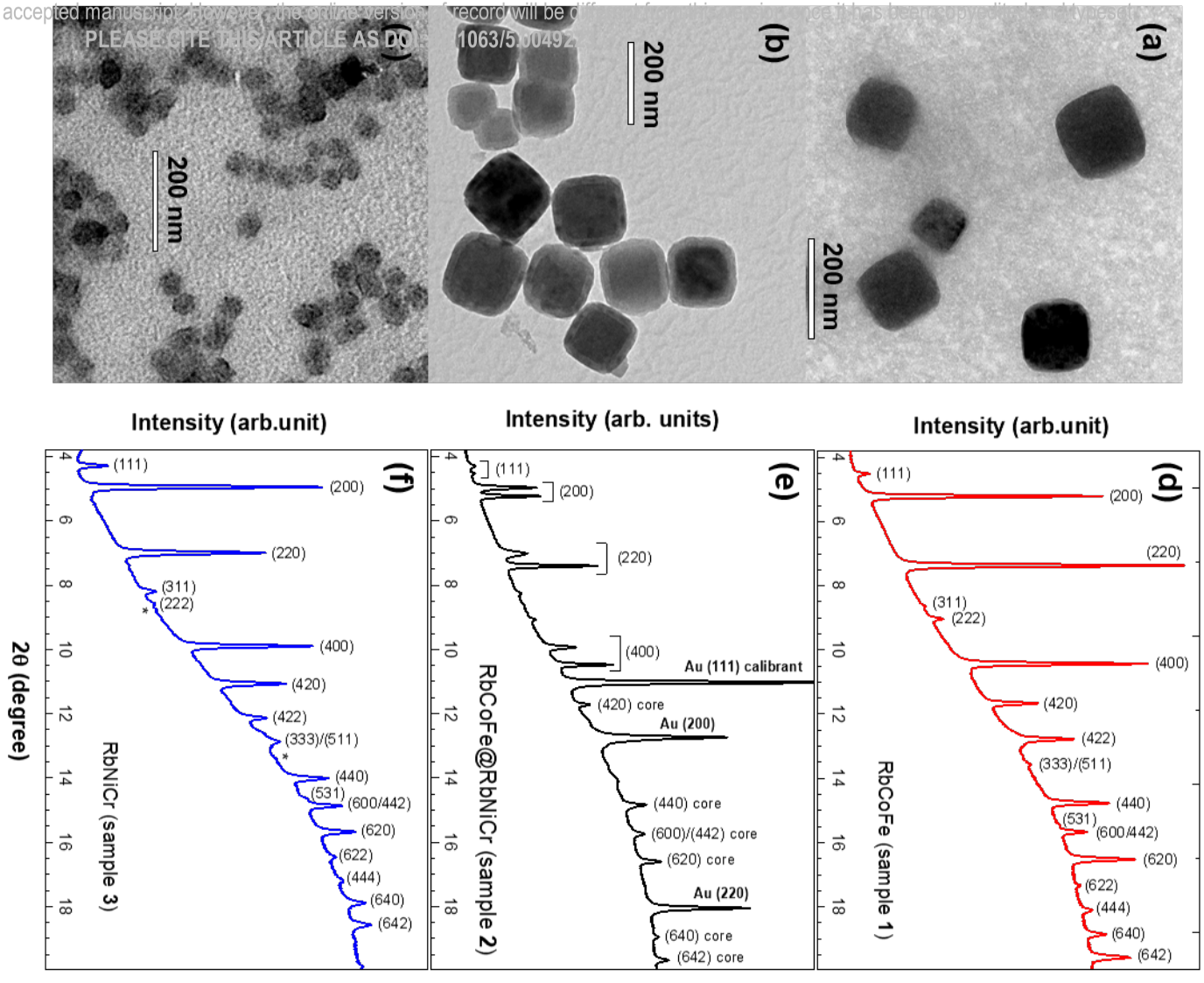

Journal of Applied Physics

ACCEPTED MANUSCRIPT

This is the author's peer reviewed, accepted manuscript. However, the online version of record will be different from this version once it has been copyedited and typeset.
PLEASE CITE THIS ARTICLE AS DOI: 10.1063/5.0049223

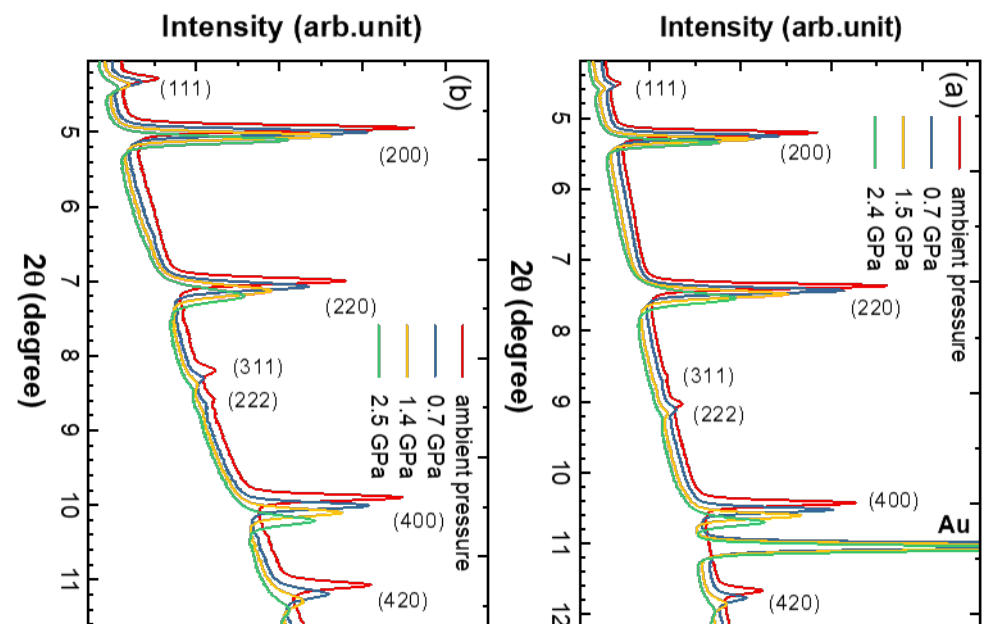

Journal of Applied Physics

ACCEPTED MANUSCRIPT

This is the author's peer reviewed, accepted manuscript. However, the online version of record will be different from this version once it has been copyedited and typeset.

PLEASE CITE THIS ARTICLE AS DOI: 10.1063/5.0045220

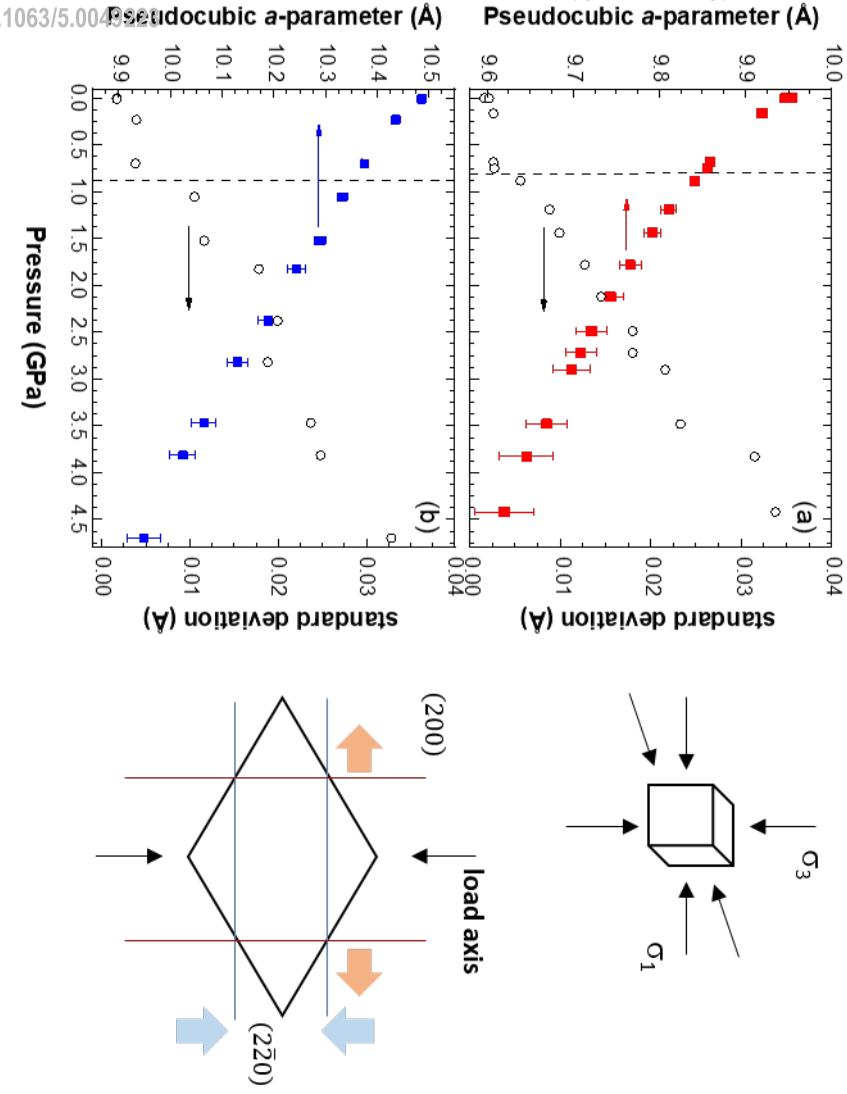

Journal of Applied Physics

ACCEPTED MANUSCRIPT

This is the author's peer reviewed, accepted manuscript. However, the online version of record will be different from this version once it has been copyedited and typeset.
PLEASE CITE THIS ARTICLE AS DOI: 10.1063/5.0049223

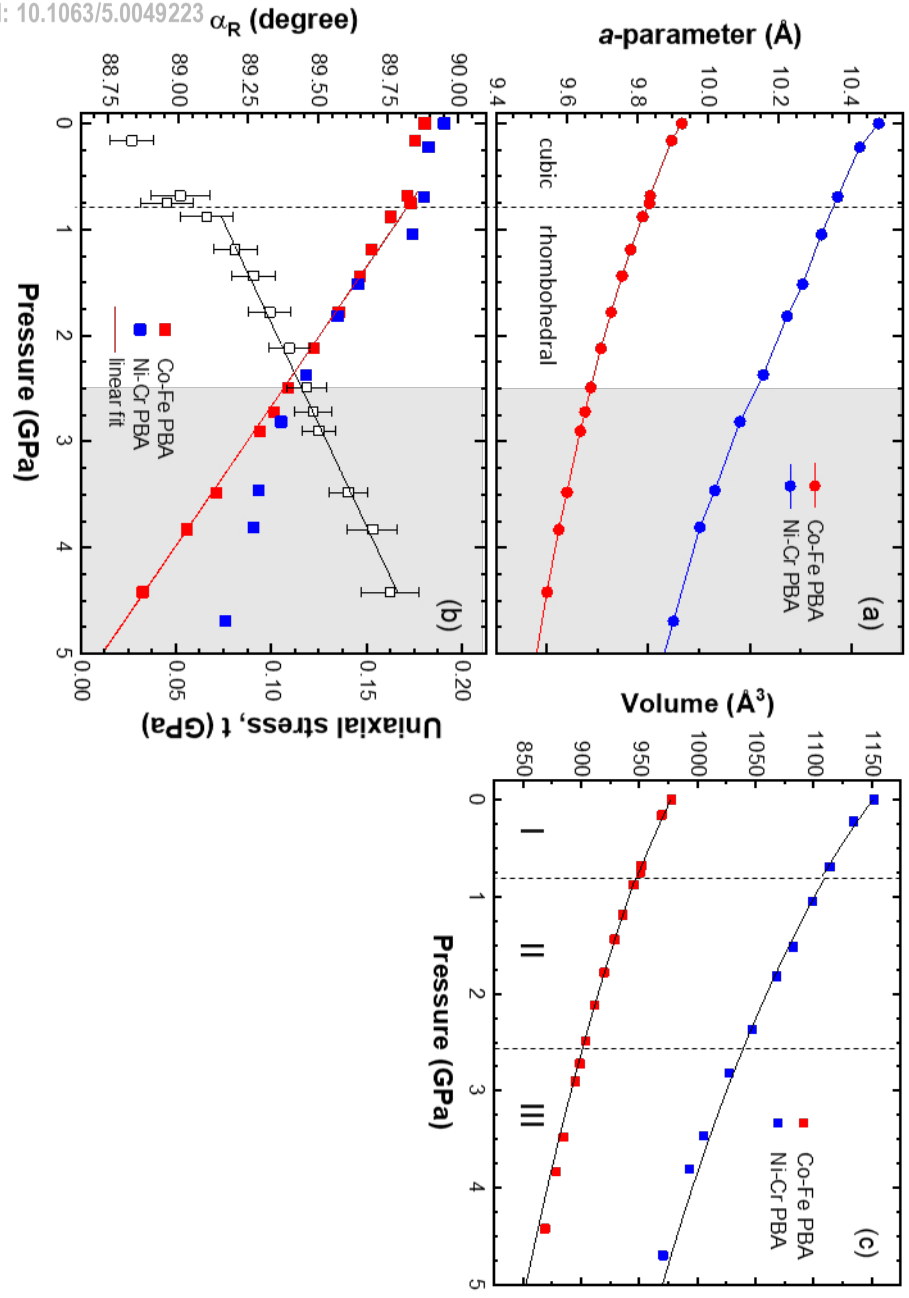

ACCEPTED MANUSCRIPT

Journal of Applied Physics

AIP Publishing
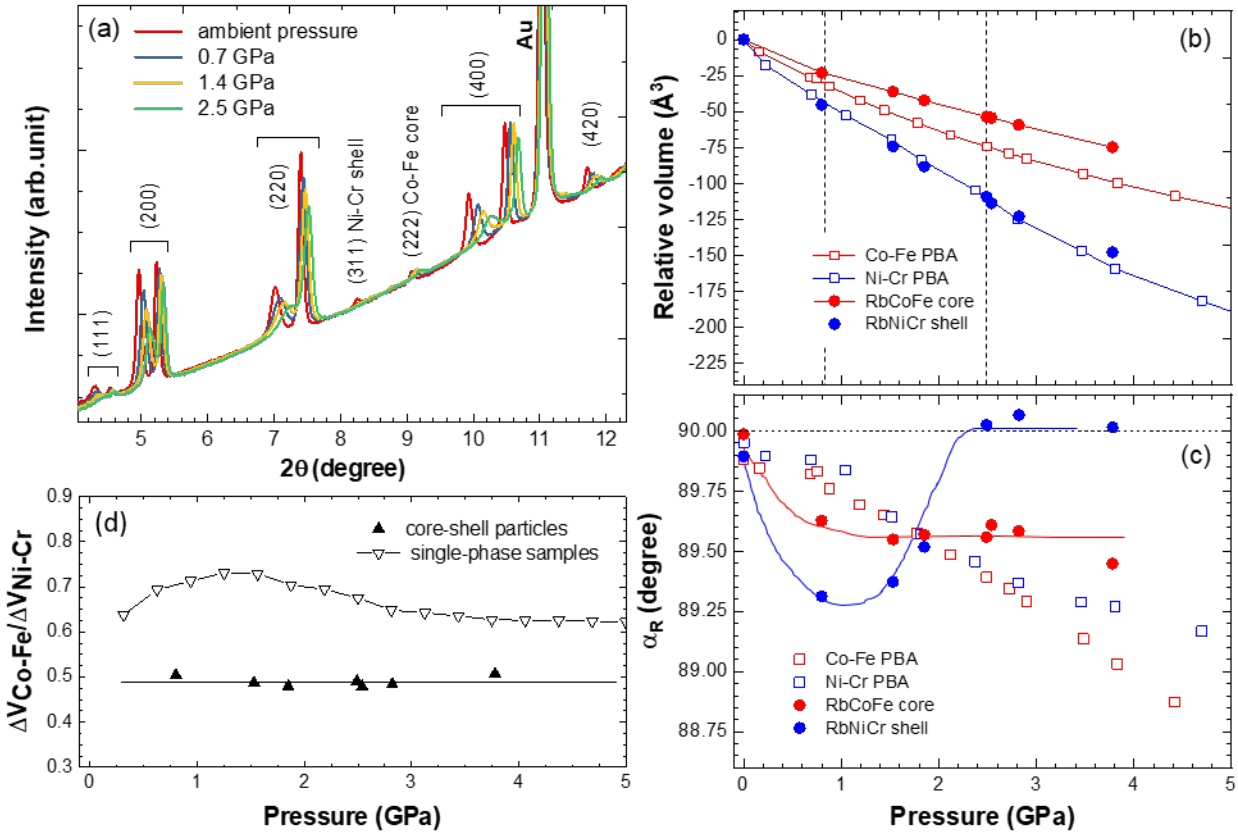
This is the author's peer reviewed, accepted manuscript. However, the online version of record will be different from this version once it has been copyedited and typeset.
PLEASE CITE THIS ARTICLE AS DOI: 10.1063/5.0049223